

A Numerical Method for Burnback Analysis of UV-cured Solid Rocket Propellant Grains

Original

A Numerical Method for Burnback Analysis of UV-cured Solid Rocket Propellant Grains / Polizzi, G., Ferrero, A., Masseni, F., Pastrone, D.. - (2024). (AIAA Scitech 2024 Orlando (USA) 8-12 January 2024) [10.2514/6.2024-0635].

Availability:

This version is available at: 11583/2984519 since: 2025-06-27T06:56:40Z

Publisher:

American Institute of Aeronautics & Astronautics

Published

DOI:10.2514/6.2024-0635

Terms of use:

This article is made available under terms and conditions as specified in the corresponding bibliographic description in the repository

Publisher copyright

AIAA preprint/submitted version e/o postprint/Author's Accepted Manuscript

(Article begins on next page)

A Numerical Method for Burnback Analysis of UV-cured Solid Rocket Propellant Grains

Giovanni Polizzi^{*}, Andrea Ferrero[†], Filippo Masseni[‡] and Dario Pastrone[§]
Politecnico di Torino, Turin, 10129, Italy

Today, numerical simulations are utilized to model the shape evolution of burning grains in solid rocket motors. These simulations can be coupled with fluid dynamic models to depict the flow field and evaluate performance. While these techniques have traditionally been applied to grains designed and produced using conventional processes, new manufacturing methods necessitate appropriate tools to simulate propellant behavior. This includes considering the new possibilities and characteristics that can be achieved with additive manufacturing. Therefore, the numerical tools used to analyze grain burn-back and the fluid dynamic field must be suitably adapted. The objective of this work is to revise existing methodologies and develop an initial version of a comprehensive tool intended for modeling nonuniform propellant burning. The distribution of propellant composition within the grain has been modeled and evaluated to assess the numerical tool's ability to accurately calculate grain burnback with a nonuniform burning rate. Representative geometries with available experimental data and numerical or analytical simulations have been considered as test cases to validate the tool. Obtained results demonstrate the tool's effective performance and its good agreement with available reference data. Additionally, the tool has proven capable of handling the nonuniform ballistic properties of the propellant.

Nomenclature

a	=	Multiplicative factor for burning rate
A_b	=	Grain burning surface
A_t	=	Nozzle throat area
c^*	=	Characteristic velocity
c_0	=	Multiplicative factor for characteristic velocity
L	=	Main axis length of the grain
m	=	Pressure exponent for characteristic velocity
\dot{m}_b	=	Mass flow of gas produced through solid propellant combustion
\dot{m}_{th}	=	Mass flow of gas expelled through nozzle
n	=	Pressure exponent for burning rate
p_c	=	Gas pressure in combustion chamber
r	=	Burning rate of the propellant
r_g	=	Radial coordinate
R_g	=	Perfect gas constant
T_c	=	Gas temperature in combustion chamber
\vec{V}	=	Velocity field of the level set equation
V_c	=	Gas volume in combustion chamber
Γ	=	Mach function for mass flow
ϕ	=	Implicit function for level set definition
ρ_b	=	Solid propellant density
ρ_c	=	Gas density in combustion chamber

^{*}PhD student, Department of Mechanical and Aerospace Engineering, Corso Duca degli Abruzzi 24, 10129 Turin, Italy

[†]Associate Professor, Department of Mechanical and Aerospace Engineering, Corso Duca degli Abruzzi 24, 10129 Turin, Italy, AIAA Member

[‡]Assistant Professor, Department of Mechanical and Aerospace Engineering, Corso Duca degli Abruzzi 24, 10129 Turin, Italy

[§]Full Professor, Department of Mechanical and Aerospace Engineering, Corso Duca degli Abruzzi 24, 10129 Turin, Italy, AIAA Associate Fellow

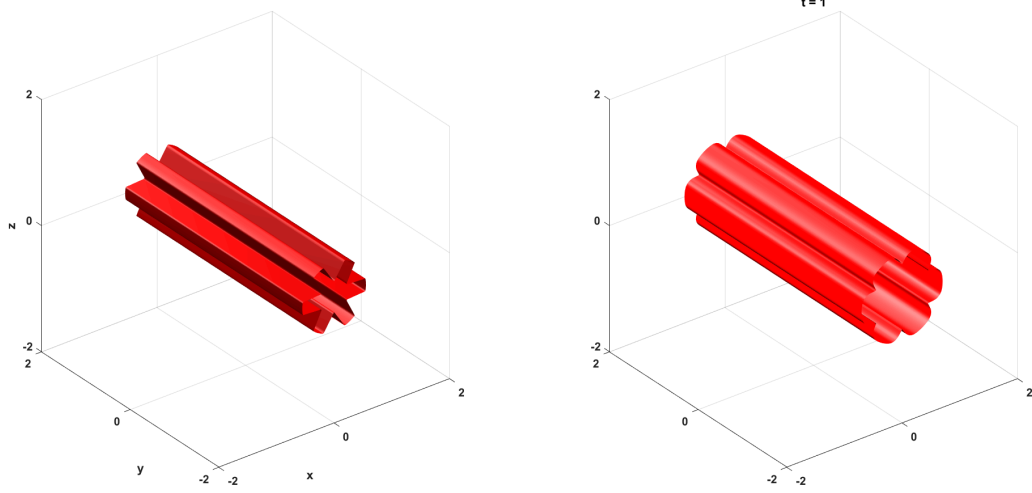
I. Introduction

Composite solid propellants are widely used in a variety of applications, spanning from civilian use (fire extinguisher, airbag systems) to aerospace propulsion (space launchers and missile systems). Solid Rocket Motors (SRMs) exploit composite solid propellant grains to produce hot gases and generate thrust; this type of propulsive system grants high thrust, high energy density, fast ignition and unmatched storage characteristics. Composite solid propellants are manufactured through a cast-cure process, aimed to obtain a solid cartridge desired mechanical and geometrical properties, which contains both fuel and oxidizer to produce hot gases through combustion process. Typically, standard materials used for grain manufacturing are Polybutadiene (PB) et similia as matrix of the composite, which acts as fuel during combustion process, loaded with high percentage (from 60% up to 90%) of Ammonium Perchlorate (AP) powder, which acts as oxidizer. Other materials are added to obtain desired performances, such as Aluminium powder (Al), Nitroamines and various additives to facilitate manufacturing process (plasticizers, wetting agents, and curing catalysts) or change mechanical and ballistic properties of the final grain (e.g. burning catalysts, retarding agents, or coolants); some of these additives are toxic chemicals, and their use is problematic, if not restricted or forbidden. For example, hydroxyl terminated polybutadiene (HTPB), one of the most used binders, is cured using multifunctional isocyanates which are toxic compounds; some of them are classified as potential human carcinogens and are known to cause cancer in animals. Furthermore, exposure to these reagents causes lung problems, asthma, and irritation of the throat, nose, eyes, and skin [1, 2]. The final shape of the grain is obtained using expendable mandrels, whose cost grows as grain geometry become more complex; moreover, particular shapes remain unattainable with mandrels, forcing design limitation for geometry and, consequentially, constraints in design phases of the motor.

An innovative approach [3] for SRM grains manufacturing, reliant on additive manufacturing techniques, is currently under development to overcome limitations of the standard process. This approach relies on UV curing of polymeric binder and grain shape casting through layer deposition. Analyses have already been carried out [4, 5] to assess the proposed process. Different polymeric binders have been tested to find most suitable ones for the desired applications. Chain polymerization has been monitored via Fourier Transform InfraRed spectroscopy (FTIR) to ensure UV curing effectiveness, Dynamic Thermal-Mechanical Analysis (DMTA) has been conducted to estimate glass transition temperature of particles loaded compound and tensile tests have assessed mechanical properties. Multi-layer samples have been produced and tested to assess layer-by-layer manufacturing and continuous deposition. Results proved that polybutadiene (PB) resins are suitable for a UV-curing manufacturing process, granting mechanical and ballistic characteristics comparable with those of samples produced with the classical cast and cure procedure. Further work is now focused on the deposition process and on new grain design approaches able to exploit the innovative process potentials.

The innovative manufacturing process offers new opportunities for grain design: first of all the possibility to overcome geometrical constraints imposed by mandrels and the possibility to control material's deposition, hence, the possibility to control material's composition inside the grain and possibly obtain a nonuniform composition, which lead to nonuniform ballistic properties. This possibility allows to increase the degrees of freedom in the grain design, allowing to change performances by altering propellant local composition. Exploring these new features requires proper computational tools, which take into account variability in ballistic properties of the propellants.

Nowadays numerical methods, such as Level Set Method (LSM) or Lagrangian markers, can be used to describe shape evolution of burning grains, coupling it with fluid dynamic models to describe flow field in the port [6–8]. These techniques, used in different fields [9], have been generally applied to grain manufactured with the classical cast and cure process. In particular, the approach here selected to track the surface burnback is based on LSM, due to its adaptability and relative ease in dealing with complex shapes attainable with innovative manufacturing techniques. Moreover, the flexibility of the method allows to easily introduce modification aimed to include the features previously described. Results here presented are based on an updated version of an existing LSM solver [10], modified to include additive manufacturing process features. Early work focused on exploiting LSM solver possibilities and to adapt its features to the specific problem, as well as finding problems and limitations of the tool. Representative geometries (i.e. star-shaped grains in Fig. 1) have been considered to test the ability of the numerical tool to evaluate parameters needed for fluid dynamic model such as burning area. Different tests have been carried out with different approximation schemes and different grid dimension. These geometries have been produced through boolean operation on primitive geometries available in LSM solver: however, this approach has proven unsuitable to address more complex geometries. Therefore, further work focused on grain shape acquisition and level set initialization through CAD modelling and meshing, as



(a) Grain surface before ignition

(b) Grain surface burnback

Fig. 1 Burnback simulation of star-shaped grain: test case 1 second

well as computing geometrical features needed for fluid dynamic model, such as burning area and combustion chamber volume. The modified tool has been then coupled with a 0D model which describes pressure evolution in combustion chamber during grain burning. This simplified model allows to couple grain burnback and chamber pressure, via the well known relation for regression rate $r = ap^n$ [11]. The coupled model has been validated on literature test cases, for which experimental and numerical data are available [12, 13]. Finally, an initial analysis of variability in ballistic performance has been carried out; the temperature coefficient a has been used to control ballistic properties distribution, allowing it to change as a function of space position inside the solid grain due to properly chosen variation of propellant composition during deposition; the possibility to control the distribution of a has been implemented, allowing to alter regression rate, hence grain performances, and behavior has been tested.

II. Initial analysis of LSM solver performances

A. LSM overview

Level Set Method is a method for tracking topological modification of curves and surfaces. It relies on the definition of an implicit function ϕ to identify and describe moving interface, its zero-level set where $\phi = 0$, and calculating its new shape at time t via so-called Level-Set Equation

$$\frac{d\phi}{dt} + \vec{V} \cdot \nabla\phi = 0 \quad (1)$$

which is a particular case of the more general Hamilton Jacobi equation. LSM is applied in different fields: image restoration and visualization, biophysics, optimization, trajectory planning, Combustion processes, CFD. As previously

mentioned, LSM could be applied to track the evolution of the grain burning surface, and monitor its shape, by imposing a velocity field \vec{V} normal to the surface and equal to propellant burning rate r . Generally speaking ϕ could be an arbitrary function, but the most efficient choice is to use the Signed Distance Field (SDF), which is the function which assign to every point in the domain the value of the distance of that point from the interface, with a positive or negative sign whether the point is outside or inside the surface, respectively. This choice allows some simplifications in numerical integration of 1 [6]

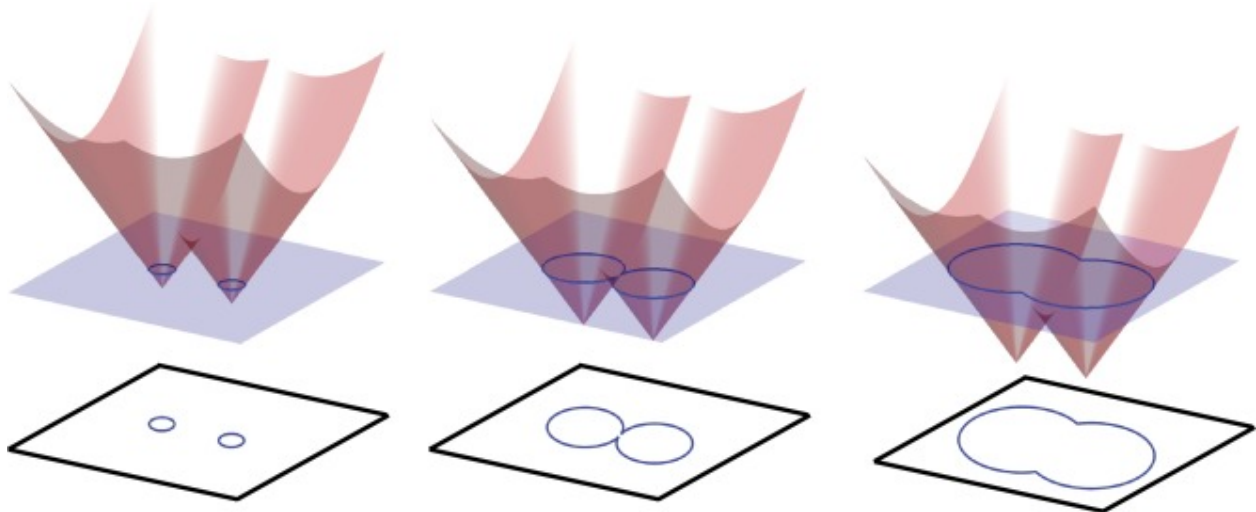


Fig. 2 LSM Visualization-2D interface visualization [9]

B. LSM solver overall description

The simulations described in this work were performed by adapting an existing LSM solver [10]. The solver includes routines for integration of Eq. 1 on an orthogonal structured grid, in different conditions. The spatial gradient of ϕ and the time integration are computed according to some numerical schemes described by [6]: Essentially Non Oscillatory (ENO) and Weighted-ENO (WENO) approximation to compute spatial reconstruction, up to fifth order accuracy, and Total Variation Diminishing Runge-Kutta (TVD-RK) for time integration. An initial analysis and comparison between different discretization schemes has been carried out but, since numerical performance of schemes is not the main topic of the work and has been already assessed in numerous dedicated works, results are not here fully reported, and further analysis are carried out using only second order accurate schemes. Different test geometries are implemented in the solver; moreover, it offers built in subroutines which allow to define and initialize simple geometries, such as spheres, cylinders or planes. Zero level surfaces are reconstructed and visualized through isosurface triangulation. However, the initial version of the software is unable to define SDF to initialize geometries for required application, thus first modifications were focused on some geometric features of the solver.

C. Basic modification and early usage

As stated above, initialization of SDF to describe desired geometries has been the first concern. First of all, a simplified test geometry has been selected to carry out initial computation. A star shaped grain has been selected for its relevance and for the possibility to compare numerical results with analytical computation of surface regression, available for this type of geometry. To initialize star shaped grain, native definition of primitive geometries has been used, and these geometries have been combined through boolean operations. Combination and definition of geometries has been controlled via geometric parameters chosen to reflect standard parameters used to define this type of geometry and to describe its evolution analytically [11]. The computation of burning area through integration of triangulation area has been implemented, and results has been compared with analytical solution 3. Comparison has been carried out with different numerical schemes and with different grid cell sizes. The performance of the solver is evaluated by means of the maximum percentage error in burning area computation during surface regression 4. It's important to

assess accuracy in area computation, since this geometric parameter has great influence in pressure integration: the preliminary results reported in this work seem promising. Finally, the velocity field is automatically set to zero when the grain surface reaches the case of the motor.

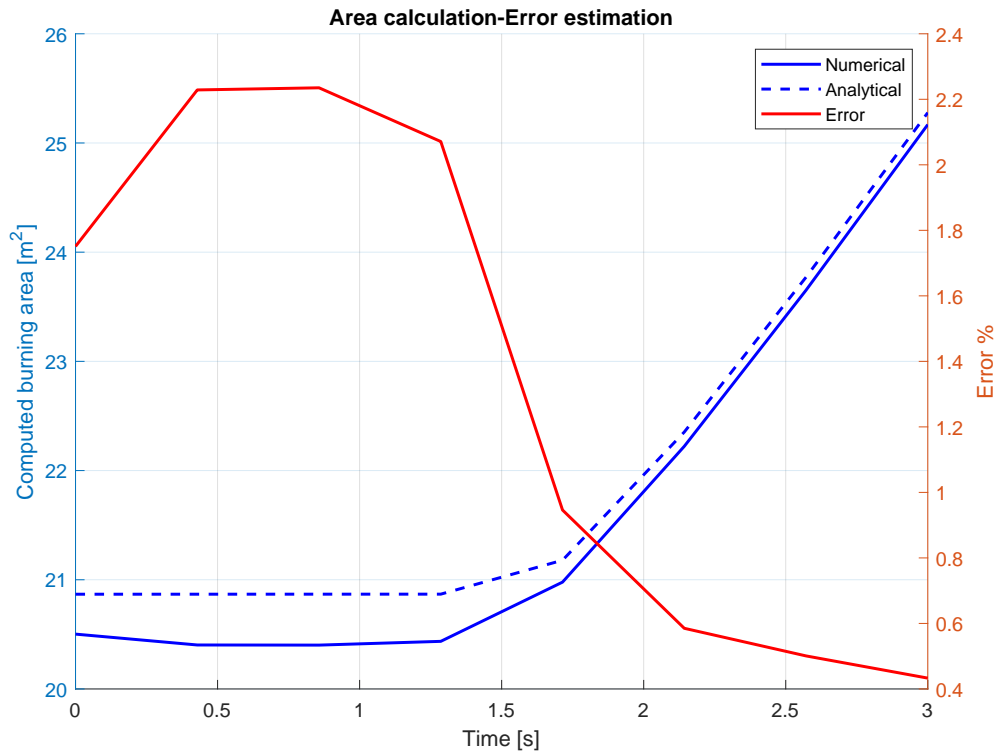


Fig. 3 Computed area and error: TVD-RK-Second Order/ENO-Second Order scheme, grid cell dimension 0.02

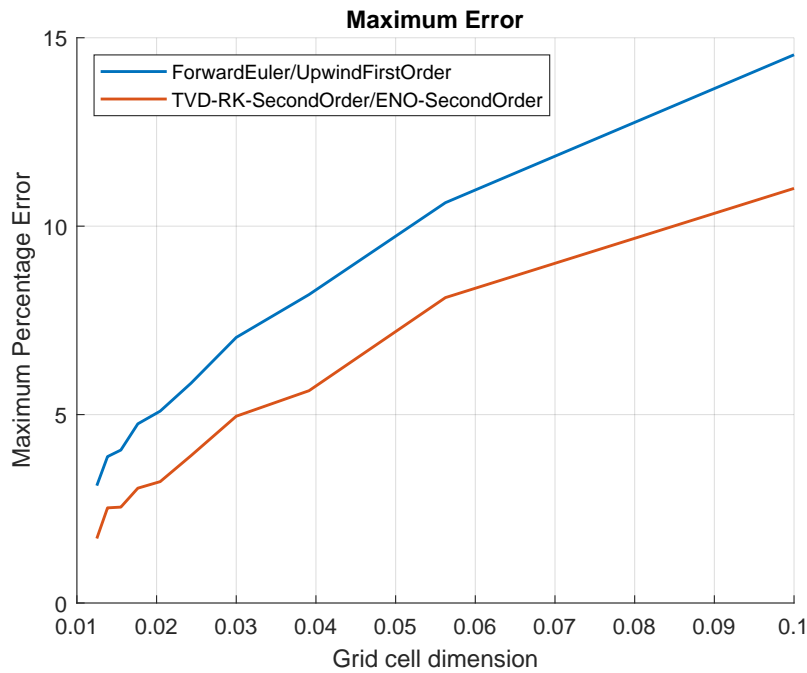


Fig. 4 Error estimation for different grid cell dimensions

III. LS Initialization from CAD modelling

A. Schematic of acquisition

Even if star shape geometry is attainable with built-in native functions, more complex geometries require a different approach to initialize SDF and integrate Level Set Equation. In fact, analytic functions to describe distance field are not available for complex geometries, hence a numerical initialization is required for these cases. To initialize SDF with a CAD-based approach, the procedure described in Figure 5 has been implemented:

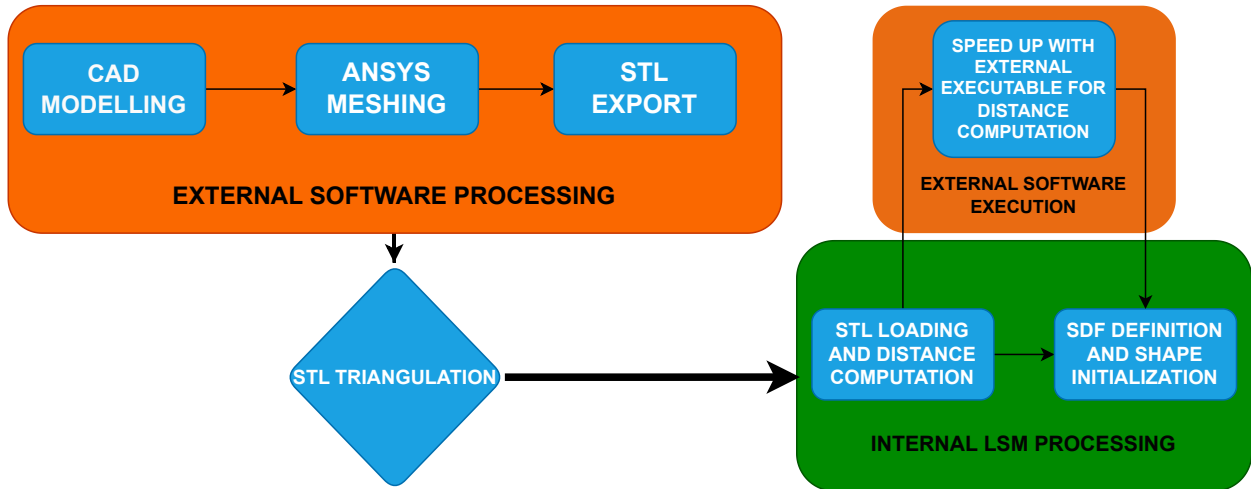


Fig. 5 Schematic representation of CAD acquisition process

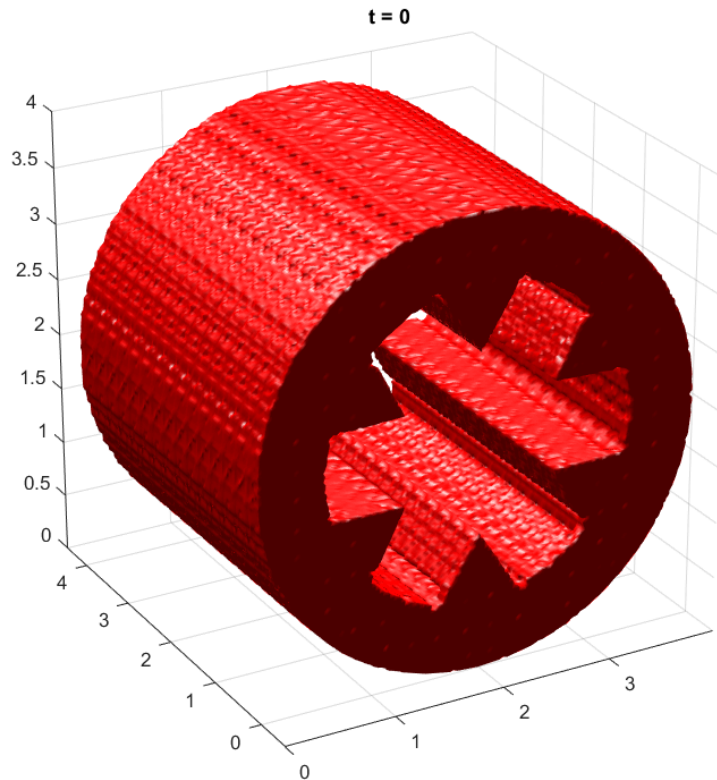


Fig. 6 Preliminary acquisition from CAD model, complete grain volume

The acquisition process relies on external software processing, which starts with CAD modelling of desired geometry. The model is then exported to a meshing software to produce a surface meshing of the model, in order to reconstruct burning area via triangulation; the latter is exported in an STL file format, and feed to LSM solver. Ad-hoc routines to read STL file and visualize and check triangulation has been implemented, and coupled with a distance field calculator: for every point of computational grid previously generated, nearest distance from triangulation (i.e. from nearest feature of nearest triangle [14]) is computed and the correct sign is assigned evaluating whether the grid point is inside or outside surface [15]. The identification of the points in the port region also allows the computation of chamber volume. Finally, the SDF is generated and the zero level iso-surface, which corresponds to the initial grain surface, is identified.

B. Results of chosen approach

In this section, some visualizations of the obtained results has been reported for different geometries. In Figure 7 and 8 the STL surface triangulation and the zero level isosurface are reported for a finocyl grain; the first slightly differs from the latter for frontal burning modification, thus with another active surface on the frontal part of the grain. In Figure 9, the zero level isosurface for a star grain is reported.

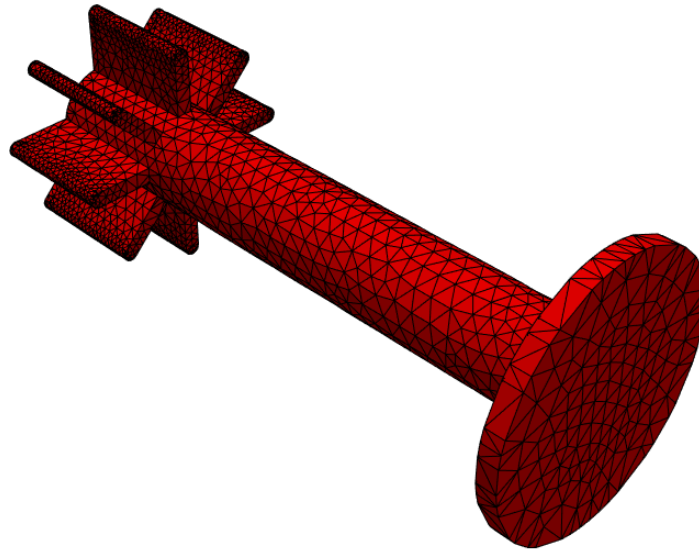


Fig. 7 STL triangulation visualization for tested finocyl geometry, with front burning modification

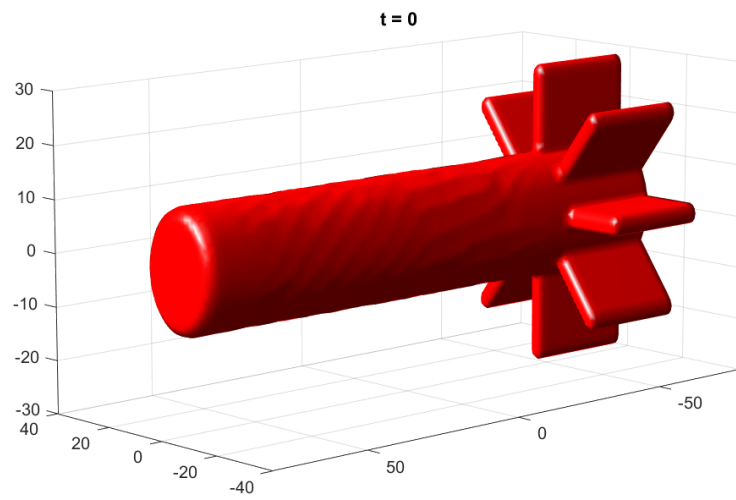


Fig. 8 Zero Level Isosurface visualization, reconstructed from computed SDF, for tested finocyl geometry

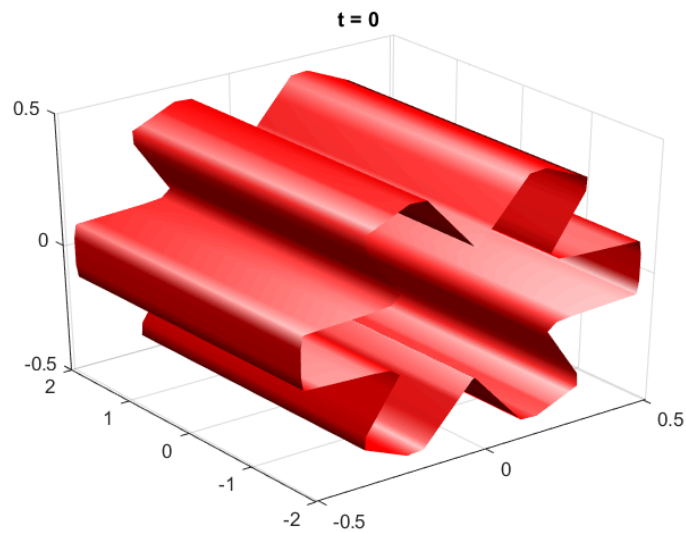


Fig. 9 Star shaped grain initialized through CAD acquisition

IV. 0D pressure model

Grain burnback simulation has been initially carried out imposing a uniform burning rate r . However, the main focus of this work is to couple shape modification with chamber flow evolution and, in particular, with chamber pressure p and assess mutual influence between the latter and burning rate, via the equation $r = ap^n$. In order to evaluate pressure inside combustion chamber, a simple 0D model has been implemented, which relies on the main hypothesis of a spatially constant value of pressure, which remains a function of time $p(t)$. This simple model allows a relatively fast way, given geometrical features evaluated thanks to burnback analysis, to evaluate pressure time history.

A. Model description

The 0D model relies on mass conservation in combustion chamber. Pressure evolution is dependent on balance between mass flow of produced gas \dot{m}_b thanks to combustion processes and mass flow expelled through nozzle \dot{m}_{th} . A complete description can be found in [11].

The mass flow rate produced by burning can be written as

$$\dot{m}_b = \rho_b A_b r \quad (2)$$

The mass conservation equation can be written as

$$\dot{m}_b = \rho_b A_b r = \dot{m}_t + \frac{d(\rho_c V_c)}{dt} \quad (3)$$

where the mass flow rate through the throat \dot{m}_t can be evaluated as

$$\dot{m}_t = \frac{p_c A_t}{c^*} \quad (4)$$

exploiting c^* definition. If an ideal gas mixture is considered then the time derivative in Eq. 3 can be rewritten as

$$\frac{d(\rho_c V_c)}{dt} = V_c \frac{d\rho_c}{dt} + \rho_c \frac{dV_c}{dt} = \frac{V_c}{R_g T_c} \frac{dp_c}{dt} + \rho_c A_b r \quad (5)$$

Hence

$$r \rho_b A_b = \frac{p_c A_t}{c^*} + \frac{V_c}{R_g T_c} \frac{dp_c}{dt} + \rho_c A_b r \quad (6)$$

The characteristic velocity can be evaluated according to the ideal rocket model: $c^* = \frac{\sqrt{R_g T_c}}{\Gamma}$. As a result, the pressure derivative is

$$\frac{dp_c}{dt} = \frac{(c^* \Gamma)^2}{V_c} (\rho_b A_b r - \frac{p_c A_t}{c^*}) = R(p_c, Geometry) \quad (7)$$

This ordinary differential equation (ODE) can be integrated provided that burning area A_b and chamber volume V_c , are available: these variables are computed through the LS equation. Time integration was performed by an implicit scheme which has been implemented as described in the next section.

B. Implicit numerical scheme for integration

The first attempts to integrate Eq. 7 has been carried out with an explicit Euler scheme, but stability limits on the time step size suggested to shift to an implicit scheme.

From Eq. 7, the time derivative can be approximated implicitly as

$$\frac{dp_c}{dt} \approx \frac{p_c^{k+1} - p_c^k}{\Delta t} = R(p^{k+1}, Geometry) \quad (8)$$

The second term in the expansion can be expanded through a Taylor approximation, computing the Jacobian $\frac{\partial R}{\partial p_c}$. Here geometrical features are considered frozen at previous time step k . In a similar way, pressure is considered frozen during geometry integration through level set. The time step Δt is the same between LS and pressure integration. With these assumptions it is possible to write:

$$\frac{p_c^{k+1} - p_c^k}{\Delta t} = R(p^k, Geometry) + \frac{\partial R}{\partial p_c}(p_c^{k+1} - p_c^k) \quad (9)$$

Solving for p^{k+1} leads to

$$p_c^{k+1} = p_c^k + \frac{R(p_c^k, Geometry)}{\beta} \quad (10)$$

$$\beta = \frac{1}{\Delta t} - \frac{\partial R}{\partial p_c}$$

The computation of Jacobian requires some consideration. If the burning rate is uniform of the grain surface than it is straightforward to compute derivatives and in this simple case the Jacobian is expressed as follows

$$\frac{\partial R}{\partial p_c} = \frac{(c_0\Gamma)^2}{V_c} [\rho_b A_b a (2m+n) p_c^{2m+n+1} - \frac{A_t}{c_0} (m+1) p_c^m] \quad (11)$$

However, things are more complex when a nonuniform burning rate is considered. Since r varies on the surface, the computation of the burned gas mass flow rate requires integration over burning surface. This is done by adapting the subroutines used to compute burning area, modified in order to assign to every triangle of the isosurface a proper value of r . Since the burning rate is defined in every point of the grid, the easiest choice is to assign the value of the nearest point of the grid to the triangle barycenter. As a result, the burning mass flow rate is computed as

$$\dot{m}_b = \rho_b p_c^n \sum_{i=1}^N A_{b_i} a_i \quad (12)$$

where N is the number of triangles of the isosurface and propellant density and gas pressure are assumed uniform. This computation allows to compute the term R and its derivative with respect to pressure:

$$\frac{\partial R}{\partial p_c} = \frac{(c_0\Gamma)^2}{V_c} [(2m+n) p_c^{2m+n+1} \Lambda - \frac{A_t}{c_0} (m+1) p_c^m] \quad (13)$$

$$\Lambda = \rho_b \sum_{i=1}^N A_{b_i} a_i$$

C. Test cases and numerical results

The coupled LS and chamber models have been tested on different configurations. First, the same star shaped grain used to evaluate area computation has been studied, in order to obtain $p(t)$ curve. Then, tests have been performed on a finocyl geometry, described in [12], where a numerical and experimental investigation of the grain are reported. The finocyl geometry has been then modified to account for front surface inhibition and different behavior has been assessed.

In Figure 10 the $p(t)$ curve for star shaped grain is reported. The overall behavior of the grain is adequately simulated, with an initial phase of neutral burning until star points disappear, and then a progressive burning until the surface reaches the case and stops burning, causing a sudden drop in pressure. However, small oscillations in the neutral phase are present, due to area estimation errors, which force pressure value to oscillate. Since these errors are directly linked to grid size, refining the grid leads to an improvement on the pressure curve, as shown in Figure 4. Figure 11 shows results for finocyl geometry which are compared to available data from literature. The comparison shows good accuracy of the solver, for simulating overall behaviour of grain propellant burning. However, there are some discrepancies with respect to experimental data: in [13] these discrepancies are supposed to be related to improper inhibition of grain front end. For this reason a modified finocyl geometry, showed in Figure 7, has been considered to simulate to evaluate the behaviour of a front burning finocyl grain. Numerical results for this geometry has been reported in Figure 11 and seem to confirm this hypothesis since the results for the front burning grain are significantly closer to the experimental data with respect to the numerical results related to the grain with the inhibited front face.

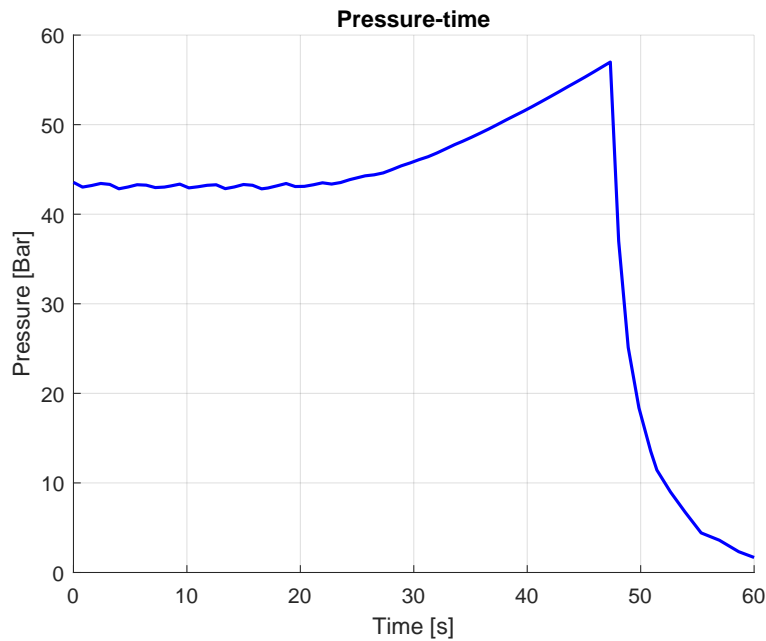


Fig. 10 Pressure time curve for star shaped grain

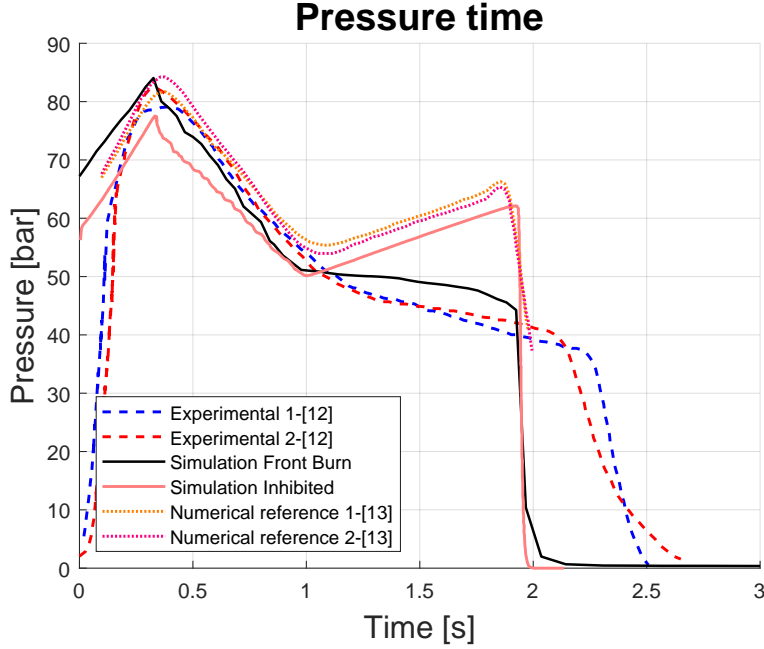


Fig. 11 Comparison with literature data, finocyl grain

It's important to consider that the implemented 0D pressure model does not describe the ignition transient since igniter behavior and flame spreading are neglected. The simulation starts at equilibrium pressure, when all initial surface started burning, and then proceeds to evaluate new pressure as the surface moves and change its geometrical features. For these reasons, experimental data of ignition transient can not be matched, and this influences the global pressure-time curve.

V. Nonuniform ballistic properties

Once pressure integration has been tested, further work was dedicated to assess the capability of the numerical tool to simulate grains characterized by nonuniform properties, in order to deal with the possibilities offered by innovative manufacturing processes.

A. Methodology

Nonuniform ballistic properties were considered by assuming a spatially varying coefficient a in the regression rate equation. With this choice, the pressure exponent n remains unaltered and so combustion stability is preserved. As a first attempt, a is described as a function of the relative radial coordinate $r_{gr\ell}$ (i.e. distance from motor casing); calling $r_{g,casing}$ absolute radial position of the casing, measured from grain main axis, relative radial coordinate is computed from absolute coordinate as $r_{gr\ell} = r_{g,casing} - r_g$. In particular, the following polynomial law has been chosen

$$a(r_{gr\ell}) = \frac{a_k}{r_{g,casing}^b} r_{gr\ell}^b + a_c \quad (14)$$

which allows some control of the distribution through adequate choice of coefficients a_k and a_c and exponent b . In 12the distribution has been plotted with respect to the absolute radial coordinate r_g . The coefficients have been tuned to provide significant ballistic properties variation. This distribution has been applied to previously studied finocyl geometry, and results are reported in Figure 14. The reduction of the initial reaction rate reduces the mass

produced during burning, hence the combustion chamber pressure is lower with respect to the previous case; the lower chamber pressure and a slowing burning, due to ballistic properties variation with radial coordinate, lead to prolonged functioning of the motor. These results show the ability to deal with nonuniform ballistic properties and how same geometry performances can be heavily altered using new possibilities of additive manufacturing techniques

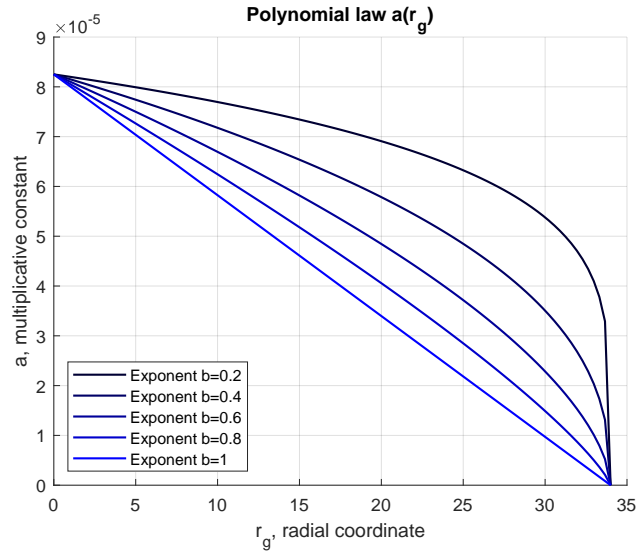


Fig. 12 Testing distribution for ballistic properties, exponent variation with $a_c = 0$ and $a_k = 8.25 \times 10^{-5}$

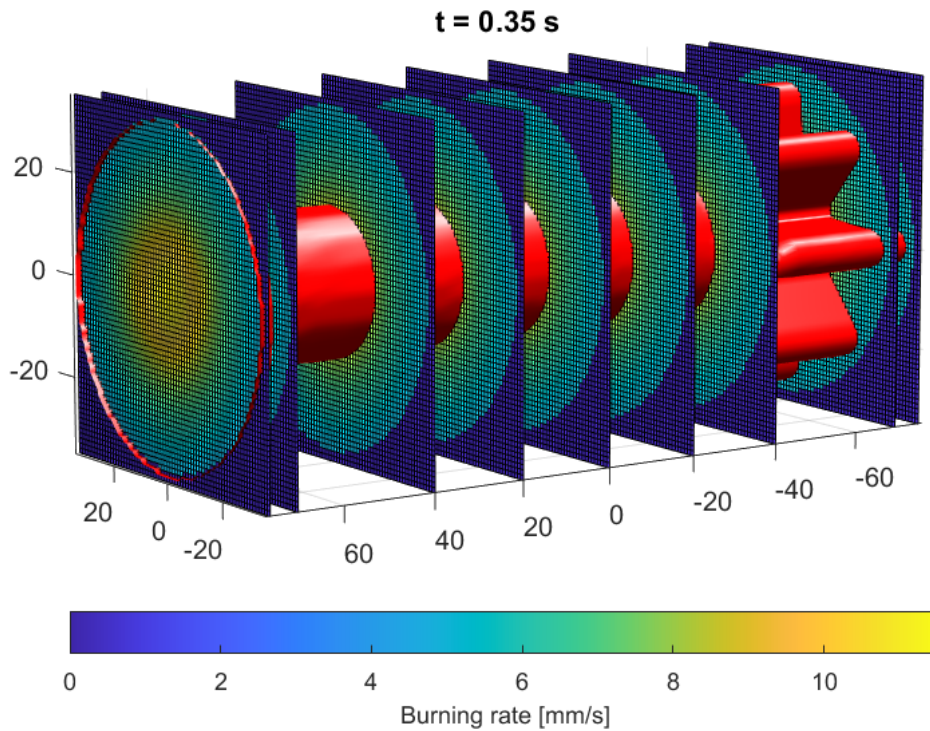


Fig. 13 Visualization of ballistic properties distribution during burnback simulation

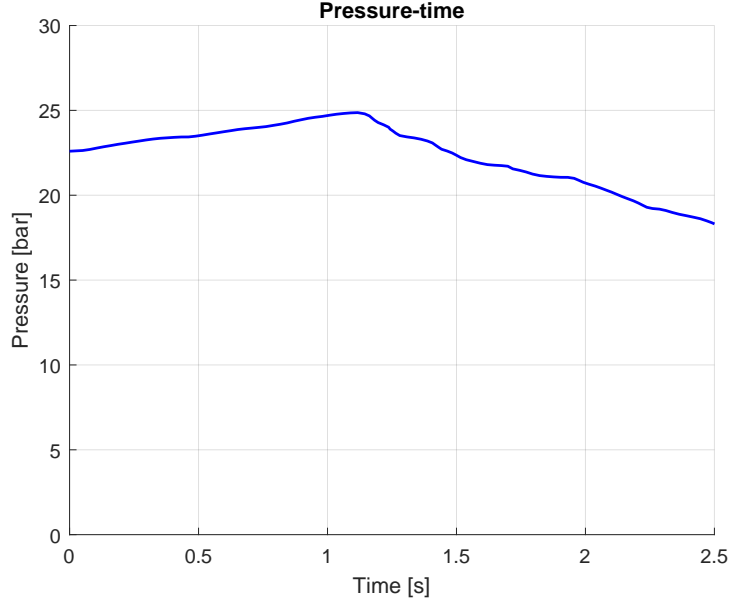


Fig. 14 Modified pressure time performance for nonuniform finocyl grain

B. Preliminary applications

After the preliminary test described in the previous Section, several possible configurations are considered. In particular, one of the goal is to obtain a cylindrical grain with neutral behavior. In order to obtain neutral burning, the following condition must be verified

$$\frac{dp_c}{dt} = \frac{(c^*\Gamma)^2}{V_c} (\rho_b A_b r - \frac{p_c A_t}{c^*}) = 0 \quad (15)$$

This means that the burning rate must vary to compensate for growing burning area. In this case r_g is the absolute radial coordinate (i.e. radial distance from motor axis). Rearranging Equation 15 and using previous relations leads to

$$a(r_g) = \frac{A_t}{c_0} \frac{p_c^{1-m-n}}{\rho_b 2\pi L} \frac{1}{r_g} \quad (16)$$

which shows how a hyperbolic distribution of a is needed to obtain neutral burning, at a certain chamber pressure, which could be arbitrary chosen. In fact, while usually equilibrium pressure is a consequence of a given geometry and propellant's ballistic properties, this problem requires finding the latter's distribution, given grain geometry and chamber pressure, which is now a design constraint. The obtained results are reported in Figure 14. Once again, the overall desired behavior is observed, but numerical errors in the computation of the burning area cause oscillations in the pressure history: the oscillations are amplified from the fact that the selected a distribution provides neutral behavior for the exact burning area, not for the numerical area affected by the integration error.

Another test was dedicated to obtain a dual thrust cylindrical grain. This was done by defining piece-wise hyperbolic functions to describe the coefficient a and divide the grain behavior in two sections, defining a particular radial coordinate at which pressure shifting must occur. The analytical for of the a distribution remains the same, only the desired constant pressure changes between the two sections

$$\begin{cases} a(r_g) = \frac{A_t}{c_0} \frac{\rho_c^{1-m-n}}{\rho_b 2\pi L} \frac{1}{r_g} & r < r_{shift} \\ a(r_g) = \frac{A_t}{c_0} \frac{\rho_c^{1-m-n}}{\rho_b 2\pi L} \frac{1}{r_g} & r \geq r_{shift} \end{cases} \quad (17)$$

Results showed in 15 shows similar limitations to previous case, especially for the first phase before shifting, but overall performance match desired behavior, with two levels of constant pressure during operation.

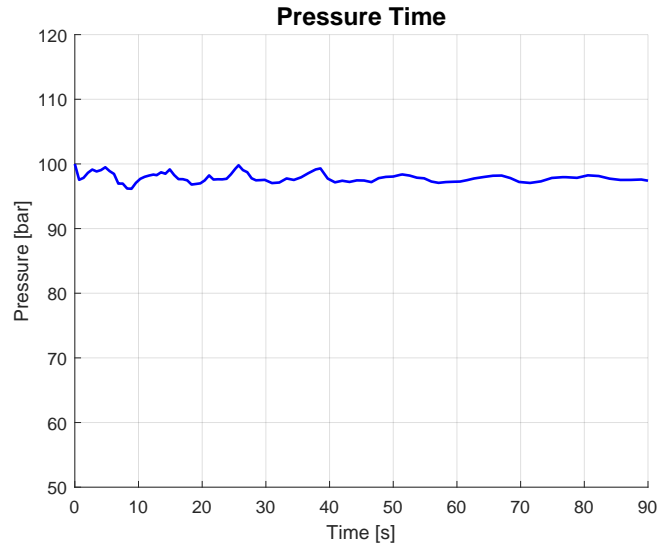


Fig. 15 Pressure Time for cylindrical shape modified for neutral burning

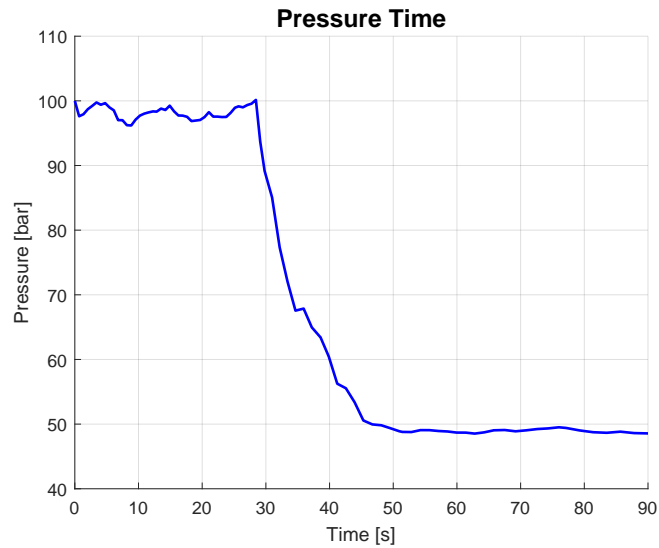


Fig. 16 Pressure time of a cylindrical shape modified for dual thrust, between 100 bar and 50 bar

VI. Conclusion and further work

In conclusion, this work has successfully achieved its principal objective by extending and adapting a numerical tool for LS integration, which has been extended and adapted for burnback analysis of generally shaped SRM grains. The enhancements include implementing geometry acquisition from CAD and initialization, computation of main geometry features, coupling with a simple model for chamber pressure evolution, and implementation of nonuniform distributions of propellant ballistic properties. The tool performance has been tested against literature numerical and experimental data as well as analytical solutions, showing good agreement and reasonable performance modification with analytical ballistic properties distributions. The tool represents a starting point to predict the behavior of nonuniform propellant grains and to explore the possibilities offered by UV curing and additive manufacturing of grains. While obtained performances are satisfactory for an initial approach, it's important to address the limitations of the present work. These limitations include errors in geometrical features computation, responsible for pressure oscillations, which can be simply reduced by refining the computational mesh. There are other limitations in the OD model, related to neglecting erosive burning or flame spreading during ignition transient. Furthermore, in the simulations with nonuniform ballistic properties, further analysis must be carried out: the final goal is to automatically compute the ballistic properties distribution in order to achieve a required thrust-time profile. Last but not least, practical feasibility of nonuniform distribution must be addressed, improving manufacturing technique readiness and evaluating suitable propellant compositions. Ongoing activities in the manufacturing process may introduce constraints on propellant production that need to be accounted for during design and simulation. To enhance this work and overcome these limitations, further activities will focus on improving accuracy of geometrical features computation, implementing and coupling higher confidence fluid dynamic models, implementing performance matching optimization of grain ballistic properties and geometry as well as conducting further studies on possible limitations of manufacturing process. This comprehensive approach aims to better understand and predict the strengths and weaknesses of this novel manufacturing paradigm.

References

- [1] Anon, W. H. O., International Agency for Research on Cancer, "IARC Monographs on the Identification of Carcinogenic Hazards to Humans," , 2022. URL <https://monographs.iarc.fr/agents-classified-by-the-iarc/>, [Online; accessed 18/10/2022].
- [2] Bolognesi, C., Baur, X., Marczyński, B., Norppa, H., Sepai, O., and Sabbioni, G., "Carcinogenic Risk of Toluene Diisocyanate and 4, 4'-methylenediphenyl Diisocyanate: Epidemiological and Experimental Evidence," *Critical Reviews in Toxicology*, Vol. 31, No. 6, 2001, pp. 737–772. doi:10.1080/20014091111974.
- [3] Pastrone, D., Sangermano, M., Garino, S., and Maggi, F., "Composite propellant manufacturing process based on deposition and light-activated polymerization for solid rocket motors," *Patent No. 102019000005788*, 2021.
- [4] Garino, S., Antonaci, P., Pastrone, D., Sangermano, M., and Maggi, F., "Photo-polymerization for additive manufacturing of composite solid propellants," *Acta Astronautica*, Vol. 182, 2021, pp. 58–65.
- [5] Galavotti, A., Noè, C., Polizzi, G., Antonaci, P., Maggi, F., Masseni, F., and Pastrone, D., "Solid Rocket Propellant Photo-Polymerization with an In-House LED-UV Prototype," *Polymers*, Vol. 15, No. 7, 2023, p. 1633.
- [6] Stanley Osher, R. F., *Level Set Methods and Dynamic Implicit Surfaces*, Applied Mathematical Sciences, Springer New York, NY, 2003.
- [7] Adel, H., and Belal, H., "Application of the level set method in solid propellant grain burnback with dogbone grain as a case study," *International Conference on Aerospace Sciences and Aviation Technology*, Vol. 19, The Military Technical College, 2021, pp. 1–15.
- [8] Wei, R., Bao, F., Liu, Y., and Hui, W., "Combined acceleration methods for solid rocket motor grain burnback simulation based on the level set method," *International Journal of Aerospace Engineering*, Vol. 2018, 2018.
- [9] Gibou, F., Fedkiw, R., and Osher, S., "A review of level-set methods and some recent applications," *Journal of Computational Physics*, Vol. 353, 2018, pp. 82–109.
- [10] Mitchell, I. M., "The flexible, extensible and efficient toolbox of level set methods," *Journal of Scientific Computing*, Vol. 35, 2008, pp. 300–329.
- [11] Sutton, G. P., and Biblarz, O., *Rocket propulsion elements*, John Wiley & Sons, 2016.

- [12] Püskülcü, G., and Ulas, A., “3-D grain burnback analysis of solid propellant rocket motors: Part 1–ballistic motor tests,” *Aerospace Science and Technology*, Vol. 12, No. 8, 2008, pp. 579–584.
- [13] Püskülcü, G., and Ulas, A., “3-D grain burnback analysis of solid propellant rocket motors: Part 2–modeling and simulations,” *Aerospace Science and Technology*, Vol. 12, No. 8, 2008, pp. 585–591.
- [14] Jones, M. W., “3D distance from a point to a triangle,” *Department of Computer Science, University of Wales Swansea Technical Report CSR-5*, 1995, p. 5.
- [15] Bærentzen, J., and Aanæs, H., “Generating signed distance fields from triangle meshes. 2002,” *Informatics and Mathematical Modeling, Technical University of Denmark, DTU*, Vol. 20, 2002.